A COMPARATIVE ANALYSIS OF MARS ODYSSEY GRS ELEMENT ABUNDANCES AND TES DUST AND MINERALOGY VARIATIONS. B. C. Hahn[1], S. M. McLennan[1], and the GRS Science Team[2]; [1]Department of Geosciences, Stony Brook University, Stony Brook, NY 11794-2100 (e-mail: bhahn@mantle.geo.sunysb.edu; Scott.McLennan@sunysb.edu), [2]Lunar and Planetary Laboratory, University of Arizona, Tucson, AZ 85721.

Introduction: The Mars Odyssey Gamma-Ray Spectrometer (GRS) instrument package has returned maps of the Martian surface for a suite of elements (i.e., refined data for Fe, Si, H, Cl, K, and Th; preliminary data for Al and Ca) [1]. An inherently low-resolution instrument, GRS has an areally extensive footprint of approximately 270 km radius and as such, gamma-ray data are best suited for analysis of large-scale geologic features or global-scale systems (e.g., analyses across the primary geologic age provinces [2], comparisons of the two TES-derived surface type end members [3], differences in Fe content between the northern lowlands and southern highlands [1,4]). GRS possesses a superior penetration depth (tens of centimeters) compared to spectroscopic instruments such as TES, THEMIS, or OMEGA, and is less sensitive to interference from thin surface dust deposits. However, these spectroscopic data sources provide specific mineralogical information and comparisons between mineralogical and chemical abundances are vital for understanding the composition and evolution of the Martian crust-mantle system.

Here we analyze GRS-derived global elemental abundances with respect to several TES-derived mineralogies and surface dust abundances. While several spectroscopic instruments capable of detecting specific mineralogies have been or are currently in operation around Mars, data supplied by the Thermal Emission Spectrometer (TES) instrument provides the global coverage and a lower resolution more easily compared to GRS data.

Data Sources and Processing: We run pixel-by-pixel comparisons between GRS Fe, Si, H, Cl, K, Th, Al, and Ca abundances and selected TES mineralogies. The GRS pixels used for this study were derived from a 2-degree base map smoothed with a 10-degree arc-radius mean filter. These are then rebinned into datasets consisting of 5º×5º bins, which have good counting statistics and provide the large number of bins necessary for improving confidences. An "H-mask" [1] has been applied to the Fe, Si, H, Cl, Al, and Ca datasets, excluding data pole-ward of ~±45º-60º latitude. This is due to interference in detecting these elements in high H abundance regions. Likewise, data for K and Th have been excluded pole-ward of ±75º due to dilution effects from large quantities of surface or near-surface water ice.

We smoothed publicly available 1º×1º mineralogical maps from the TES Science Team website to a 5º×5º pixel resolution to allow comparison with the GRS data [5]. We limit ourselves to only the TES datasets designated: Surface Dust, High-Calcium Pyroxene, Sheet Silicates/High-Si Glass, and Plagioclase. These four TES datasets are the only global-scale maps available that provide a large number of pixels registering near or above the TES detection limit at smoothed 5º×5º resolution and, therefore, are the only TES datasets likely to provide statistically robust comparisons with GRS.

Method: First, using a method similar to that employed by *Hahn et al., 2007* [2], each TES mineralogical or dust abundance dataset was divided into three categories representing High, Medium, and Low areal abundances (e.g., High, Medium, and Low Plagioclase). These three categories were determined for a particular mineralogy such that each category contains enough pixels (>100 pixels) to allow good statistics. For example, "High Plagioclase" is assigned to all 5º×5º pixels with >10% TES-determined areally abundant plagioclase (335 pixels); "Medium Plagioclase" is assigned to all pixels with 5%-10% abundances (395 pixels); and "Low Plagioclase" is assigned to pixels with <5% abundances (778 pixels). Second, elemental abundance means were determined for each mineralogical category using the GRS chemical datasets. Thus, changes in a particular elemental abundance were recorded with respect to varying mineralogies (see **Figure 1** for an example of this approach).

Further, to try to constrain the chemical composition of the Martian dust layer, we calculated chemical means for each mineralogy with varying dust abundance as determined by TES.

Martian Surface Homogeneity: Despite considerable geologic and mineralogical diversity [6], GRS data reveal a fairly chemically homogeneous Martian surface, although anomalous regions and outliers exist. This lack of chemical diversity stems from a number of factors. Mars has a basalt crust with no evidence of major regional chemical variations comparable to the lunar highlands or Earth's continents. The Martian crust has likely experienced broad-scale mixing through time by a combination of impact gardening and eolian and aqueous processes. The lack of an active plate tectonics regime prevents the recycling,

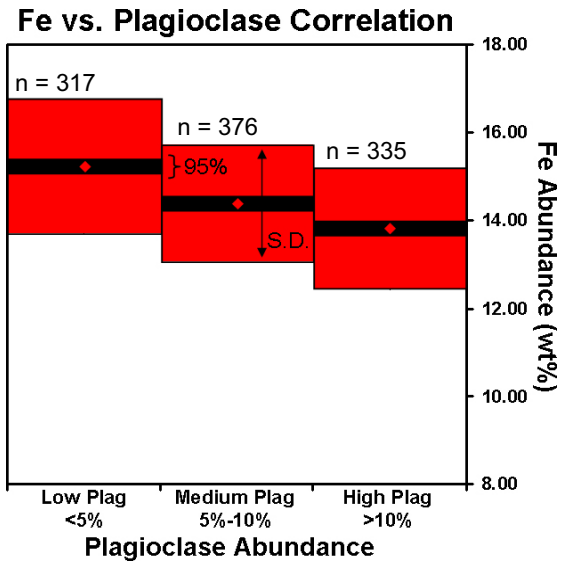

Figure 1: *Fe concentration with varying plagioclase content.* Red boxes and black bars represent the standard deviations and 95% confidence intervals, respectively, of the calculated GRS elemental abundance means for each TES mineralogical abundance category. The large number of pixels used to calculate the chemical means allows for a high level of confidence. Data were screened to exclude pixels with dust contents higher than 50%.

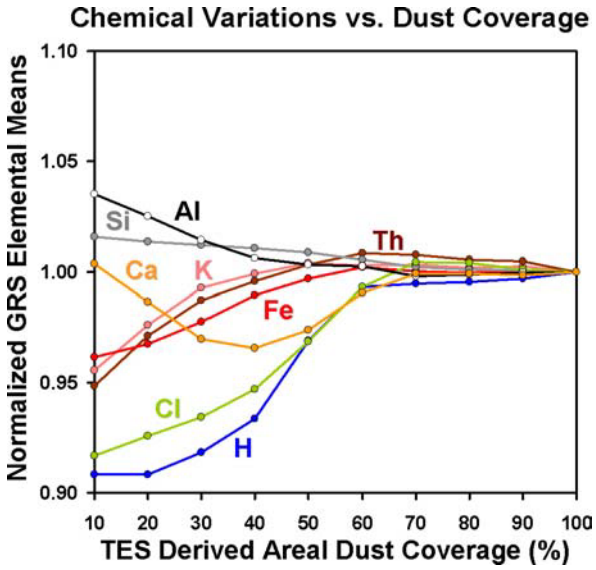

Figure 2: *Chemical variations as a function of areal dust coverage.* Points represent GRS elemental abundance means calculated from pixels for regions of a specific TES-derived dust coverage (e.g., 30% dust coverage includes all pixels with 30% or less coverage; 100% dust coverage includes all pixels with 100% or less coverage – i.e., the entire surface). Accordingly, confidence levels in the means decrease to the right as pixel numbers increase. Means are normalized to their respective global averages (i.e., 100% coverage) so that each element plots at the same scale. This approach also minimizes calibration uncertainties for the preliminary Al and Ca data.

fractionation and evolution of crustal material normally seen at active plate boundaries on Earth. Air fall dust transported globally also contributes to surface chemical homogeneity. Additionally, soil analyses from geographically separate lander missions show remarkably similar chemical signatures [7,8], with most variation attributed to a local chemical component. Performing analyses using large categories with many pixels affords us a high confidence level; however, chemical variations are often subtle. [Note also, that even statistically significant chemical variations may not have geologic significance or may be due to factors unrelated to mineralogy.]

Results: A number of chemical trends are evident using these methods of pixel by pixel comparisons. For example, as illustrated in **Figure 1**, several elements vary subtly with mineralogies. Most notably: both Fe and H decrease with increasing plagioclase abundances; Si increases with both increasing plagioclase and pyroxene abundances; both K and Th decrease with increasing pyroxene abundances; and both H and Cl decrease with increasing sheet silicates/high-Si glass abundances.

Chemical contamination from dust is also a factor with GRS data. Degree of dust coverage has a considerable effect on chemistry and clear trends can be seen. **Figure 2** shows the effects on elemental mean abundances with varying surface dust coverage. Elemental abundances (normalized to their respective global means for plotting purposed) are plotted against increasing dust coverage. Note the strong correlation of Cl and H with surface dust coverage, evidence of enrichment of these highly mobile elements.

A full statistical analysis with well-constrained errors and z-statistic tests for all mineralogical and elemental comparisons will accompany finalized data.

References: [1] Boynton W. V. et al., (2007) *JGR-Planets,* submitted. [2] Hahn B. H. et al., (2007) *JGR-Planets*, in press. [3] Karunatillake S. et al., (2007) *JGR-Planets*, in press. [4] Taylor G. J. et al., (2007) *JGR-Planets*, in press. [5] Christensen P. R. et al., (2001) *JGR-Planets*, 106, 23,823-23,871. [6] Christensen P. R. et al., (2005) *Nature*, 436, 504-509. [7] Gellert R. et al., (2004) *Science*, 305, 829-832. [8] Rieder R. et al., (2004) *Science*, 306, 1746-1749.